Hexagonal Mesoporous Titanium Tetrasulfonates with Large Conjugated Hybrid Framework for Photoelectric Conversion

Tian-Yi Ma,[†] Yan-Shuang Wei,[‡] Tie-Zhen Ren,[‡] Lei Liu,[†] Qiang Guo,[†] and Zhong-Yong Yuan*,[†]

Institute of New Catalytic Materials Science, Key Laboratory of Advanced Energy Materials Chemistry (Ministry of Education), College of Chemistry, Nankai University, Tianjin 300071, P.R. China, and School of Chemical Engineering & Technology, Hebei University of Technology, Tianjin 300130, P.R. China

ABSTRACT Ordered hexagonal mesoporous titanium tetrasulfonate materials (CuPcS$_4$–Ti) were synthesized through a hydrothermal process with the assistance of surfactant F127, by using the copper(II) phthalocyanine-tetrasulfonic acid tetrasodium salt (CuPcS$_4$) as coupling molecules. It was confirmed by TEM, IR, UV–vis, TGA-DSC, and XRD analysis that the CuPcS$_4$ groups were homogenously incorporated into the hybrid framework, and the synthesized materials could be stable to around 328 °C with the hybrid framework and ordered mesopores well-preserved. A high dye content of Ti/CuPcS$_4$ molar ratio at around 50 was achieved, which could be useful in the photoelectric conversion applications. A novel model of isolated dye centers surrounded by semiconductor oligomers was set, which could effectively suppress the aggregation of dye molecules that may decrease the conversion efficiency in some traditional dye-sensitized solar cells. It was proved that the synthesized CuPcS$_4$–Ti exhibited a relatively high conversion efficiency of 0.53 %. It was very valuable to access such a high conversion efficiency by using low-cost and commercially available dye molecules instead of using the expensive unsymmetrical phthalocyanines synthesized by the time-consuming methods in the literature.

KEYWORDS: ordered mesostructure • mesoporous • titanium sulfonate • photoelectric conversion • dye-sensitized solar cell

1. INTRODUCTION

Exhaustion of fossil fuels, such as petroleum, coal and natural gas, and reduced emission of carbon dioxide and other harmful substances have attracted more and more concerns of the global society. Solar energy is regarded as one of the most promising candidates among a variety of regenerable energy sources developed to date, among which dye-sensitized solar cells based on semiconductor membranes have been widely investigated (1). Ruthenium(II) bipyridyl complexes have proven to be the most efficient TiO$_2$ sensitizer in dye-sensitized solar cells. But considering the main drawbacks of the ruthenium-based sensitizer, namely, their lack of absorption in the red region of the visible spectrum and that ruthenium is a rare metal (2), novel dyes without metal or using inexpensive metal are desirable for highly efficient dye-sensitized solar cells. Phthalocyanines have been studied extensively because of their strong absorption ($\varepsilon = 1 \times 10^5$ M^{-1} cm^{-1}) in the far-red region of the spectrum ($\lambda \approx 680$ nm) (3), and the light harvesting and photocurrent generation properties could be benefited from the large conjugated system in their structure (4, 5). However, the well-known aggregation tendency of phthalocyanines that is considered to enhance the self-quenching of the phthalocyanine excited singlet state, as well as the poor solubility in common organic solvents, and the lack of directionality in the excited state are attributed as the main reasons impeding the revelation of their potential for use in solar cell performance (6), resulting in unimpressive photoelectric conversion efficiency for most reported phthalocyanine-sensitized cells (7–9). Recently, a kind of self-synthesized unsymmetrical phthalocyanine for red light harvesting was provided that the degree of aggregation is partially diminished by introducing three bulky t-butyl groups into the macrocycle plane, and the highest power conversion efficiency ever reported of up to 3.5 % has been achieved (10, 11). On the other hand, the traditional preparation for the dye-sensitized electrodes of solar cells is accomplished by the adsorption of dye molecules onto the presynthesized semiconductor membranes, which usually leads to a very low loading amount of the photosensitve molecules (12). The overincreasing of the loading amount would result in the dye aggregation mentioned above (6), which actually is also a waste of the high-cost dyes, because the poor contact between the aggregated dye molecules and the semiconductor could block the transmission of photoelectrons.

Metal sulfonate frameworks have been studied considerably less than other classes of hybrid materials, because of the coordination interactions between sulfonate anions and metal cations are relatively weak, which makes the networks not sufficiently robust to sustain permanent pores (13). Some dense (14), layered (15), and open-framework (16) metal sulfonates have been synthesized with nonporous or microporous structures, still suffering from many disadvan-

tages. The discovery of mesoporous materials has broken the size limitation of covalently bonded pore structure and endured the weak interactions between the coupling molecule and metal ions (17). Mesoporous materials, due to its large pore size and pore volume, have found wide applications in the areas of energy conversion (18), adsorption and separation (19), catalysis (20), etc. Noticeably, mesoporous metal oxide semiconductors such as mesoporous TiO_2 membranes have been widely used in dye-sensitized solar cells with high conversion efficiencies (21−23). Our aim was to prepare mesoporous metal sulfonate hybrid materials, which have never been accessed to the best of our knowledge. Having various organic functional groups, mesoporous metal sulfonates are expected to be another important family of mesoporous hybrid materials with a great composition variety, anchoring through S−O···Me (Me: Ti, Zr, V, Al, etc.) modes. A deeper step was to adopt sulfonate anions with specific functionality potentially useful in different fields, and the commercially available copper(II) phthalocyanine-tetrasulfonic acid tetrasodium salt ($CuPcS_4$, see Scheme S1 in the Supporting Information) was chosen as the coupling molecule herein. In this contribution, the novel ordered hexagonal titanium sulfonate materials ($CuPcS_4$−Ti) constructed from the conjugated tetrasulfonic tetrasodium salt ($CuPcS_4$) were synthesized by a autoclaving process with triblock copolymer F127 as the template. The one-pot condensation of $TiCl_4$ with $CuPcS_4$ allows the molecular-level penetration of large π-aromatic groups into the semiconductor network homogenously, resulting in an unprecedented large loading amount of organic dyes, but without the disadvantages of dye aggregation and electron ill-transmission due to the isolation of single $CuPcS_4$ centers by the surounding semiconductor oligomers. Thus the resultant mesoporous hybrids were used for photoelectric conversion under the simulated sunlight irradiation, proved to be efficient photocurrent conductors and better electrode materials than the traditional dye-modified titania materials under the same experimental conditions. This model supplies us with an alternative strategy for the construction of new dye-sensitized solar cells from organic−inorganic hybrid mesoporous materials. And the promotion space of the conversion efficiency is supposed to be very large due to the wide adjustable range of dye contents in the sulfonate hybrids. It is also the first successful example of obtaining the high conversion efficiency of 0.53 % by using low-cost dye molecules instead of the previously reported unsymmetrical highly substituted phthalocyanines.

2. EXPERIMENTAL SECTION

2.1. Materials. Titanium tetrachloride ($TiCl_4$) was obtained from Tianjin Kermel Chemical Co. Nonionic triblock copolymer F127 ($EO_{106}PO_{70}EO_{106}$) was obtained from Nanjing Well Chemical Co., Ltd. Copper(II) phthalocyanine-tetrasulfonic acid tetrasodium salt ($CuPcS_4$) was obtained from Sigma-Aldrich Chemical Co. All chemicals were used as received without further purification.

2.2. Synthesis of Ordered Mesoporous Titanium Tetrasulfonates ($CuPcS_4$−Ti). In a typical synthesis procedure, 12.6 mmol of $TiCl_4$ was added into 10 mL of ethanol at room temperature to form a transparent solution (solution A); 0.28 mmol of $CuPcS_4$ and 5.5 mmol of F127 were dissolved in 40 mL of deionized water (solution B) at 40 °C, followed by stirring for 1.5 h. Solution A was added dropwise into solution B very slowly, and the pH value of the mixture was adjusted to 4.0 by NaOH (0.001 mol/L) and HCl (0.01 mol/L) solution. The mixture was kept at 40 °C and stirred for another 6 h before sealed in one Teflon-lined autoclave and aged statically at 80 °C under autogenous pressure for 24 h. The obtained mixture was filtered and washed with ethanol and water repeatedly. And the removal of the surfactant and the unreacted $CuPcS_4$ was accomplished by the Soxhlet-extraction with ethanol for 96 h, marked as $CuPcS_4$−Ti (Ti/$CuPcS_4$ molar ratio of 50). To test the thermal stability of the ordered mesostructure, the as-prepared sample was calcined in the air at 200, 300, 350, and 400 °C, respectively. By slightly adjusting the adding amounts of the raw materials, we could also obtain a series of ordered mesoporous $CuPcS_4$−Ti materials with the Ti/$CuPcS_4$ molar ratio of 49, 51, and 52.

2.3. Characterization. Transmission electron microscopy (TEM) was measured on a Philips Tecnai G20 at 200 kV. Fourier transform infrared (FT-IR) spectra were measured on a Bruker VECTOR 22 spectrometer with KBr pellet technique, and the ranges of spectrograms were 4000 to 400 cm^{-1}. Diffuse reflectance UV−vis. absorption spectroscopy was employed on a TU-1901 spectrophotometer using $BaSO_4$ as a reference. X-ray diffraction (XRD) patterns were recorded on a Rigaku D/max-2500 diffractometer with CuKα radiation operated at 40 kV and 100 mA. X-ray photoelectron spectroscopy (XPS) measurements were performed on a Kratos Axis Ultra DLD (delay line detector) spectrometer equipped with a monochromatic Al−K$_\alpha$ X-ray source (1486.6 eV). All XPS spectra were recorded using an aperture slot of $300 \times 700 \, \mu m$, survey spectra were recorded with a pass energy of 160 eV, and high-resolution spectra with a pass energy of 40 eV. Thermogravimetry (TG) and differential scanning calorimetry (DSC) were performed using a TA SDT Q600 instrument at a heating rate of 5°/min using α-Al_2O_3 as the reference. The chemical compositions of Ti and Cu were analyzed by inductively coupled plasma (ICP) emission spectroscopy on a Thermo Jarrell-Ash ICP-9000 (N+M) spectrometer. N_2 adsorption−desorption isotherms were recorded on a Quantachrome NOVA 2000e sorption analyzer at liquid nitrogen temperature (77 K). The samples were degassed at 150 °C overnight prior to the measurement. The surface areas were calculated by the multipoint Brunauer−Emmett−Teller (BET) method, and the pore size distributions were obtained from the adsorption branch of the isotherms by the BJH (Barret−Joyner−Halenda) model.

2.4. Photoelectric Conversion. The preparation of $CuPcS_4$−Ti working electrode was achieved by mixing 0.2 g of the as-synthesized $CuPcS_4$−Ti powder with 0.5 g of water and 1.0 g of ethanol to form a homogeneous slurry. The slurry was then deposited on a transparent conductive glass to give a suitable thickness, followed by the calcination at 300 °C for 2 h. The configuration of self-made solar cell was shown in Figure S1 (Supporting Information), with $CuPcS_4$−Ti coated conductive glass as the working electrode and a graphite rod (in a columniform shape with diameter of 0.6 cm and length of 1.5 cm) as the counter electrode. The electrolyte (0.1 mol/L LiI, 0.05 mol/L I_2, 0.6 mol/L 2,3-dimethyl-1-propylimidazolium iodide, and 0.5 mol/L 4-*tert*-butylpyridine in acetonitrile) was introduced into the interelectrode cavity surrounded by insulating rubber walls. And the efficient contact area of electrolyte to $CuPcS_4$−Ti film was measured to be 0.8 cm^2. The photoelectric conversion behavior of the present solar cell was evaluated by an electrochemical analyzer (CHI660C Instruments) under AM 1.5G simulated sunlight, which was produced by a 300-W Oriel Solar Simulator (model 91160) with an illumination intensity of 100 mW cm^{-2}. The incident light intensity was calibrated by a
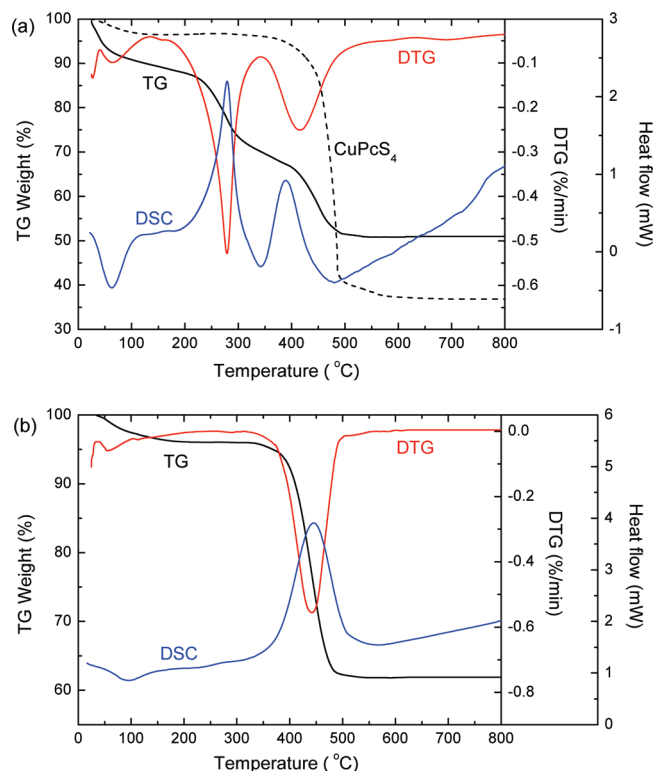
FIGURE 1. TG-DSC profiles of the as-synthesized CuPcS$_4$−Ti solid (a) before and (b) after surfactant removal, in which the dashed line denotes the TG profile of CuPcS$_4$.

FIGURE 2. Low-angle XRD patterns of the as-prepared CuPcS$_4$−Ti and calcined samples at different temperatures.

standard crystalline silicon solar cell (the 18th Research Institute of Electronics Industry Ministry, China). The overall conversion efficiency (η) of the present solar cell is determined by the short-circuit photocurrent density (J_{sc}), the open circuit potential (V_{oc}), the fill factor (ff) of the cell, and the input light irradiance (P), as shown in the following equation: $\eta = J_{sc}V_{oc}$ff/P. As a comparison, the ordered mesoporous structure of CuPcS$_4$−Ti material was destroyed by the ball milling technique before the measurement. And the CuPcS$_4$ modified titania electrode with similar pore structure and dye content to those of CuPcS$_4$−Ti based hybrid electrodes was prepared by adsorption of CuPcS$_4$ molecules onto the presynthesized mesoporous titania membrane, followed by drying and calcination at 300 °C. The photoelectric conversion behaviors under four different monochromatic light sources including ultraviolet light (390 nm), blue light (462 nm), green light (527 nm), and ed light (650 nm) were also measured by a Zennium electrochemical workstation (ZAHNER-Elektrik Gmbh & CoKG, Germany), and the input powers of the four light sources could be altered within a certain range.

3. RESULTS AND DISCUSSION
3.1. Material Synthesis and Characterization.
The good solubility of CuPcS$_4$ in water facilitates its usage for condensation with TiCl$_4$, and the one-step reaction was carried out in a mixed solution of water and ethanol (V_{water}: $V_{ethanol}$ = 4:1), similar to the reported preparation of pillared metal sulfonates (24). Removal of surfactant species was accomplished by extraction with ethanol solution at a relatively low temperature for the protection of the organosulfonate framework (25). The thermal stability of the organic moiety in the hybrid sulfonates was tested by the TGA-DSC analysis (Figure 1). The TGA curves demonstrate an initial weight loss of 10.7% from room-temperature to 155 °C, accompanying with an endothermal peak around 66 °C in
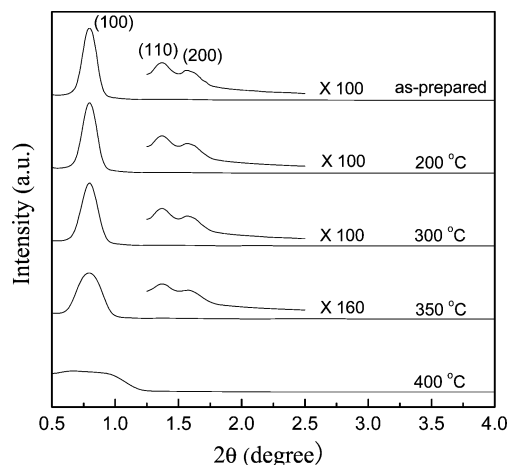
the DSC curve, which can be assigned to the desorption of the adsorbed and intercalated water. The weight loss of 18.6% from 155 to 341 °C, accompanied by an exothermic peak at around 277 °C, can be attributed to the decomposition of the surfactant. The third weight loss of 19.2% from 341 to 534 °C, accompanied by an exothermic peak at around 388 °C, can be related to the decomposition of the coupling molecule CuPcS$_4$ in the framework, which was consistent to the range of weight loss for pure CuPcS$_4$ (dash line). After surfactant removal from the sample, one weight loss of 4.8% from room-temperature to 110 °C and another weight loss of 35.2% from 328 to 540 °C, corresponding to the desorption of water and the decomposition of CuPcS$_4$ respectively, were detected, which suggested the complete removal of surfactant F127 by an ethanol extraction process. It was also denoted that the organosulfonate groups in CuPcS$_4$−Ti could be thermally stable up to around 328 °C.

The hexagonal mesophase of CuPcS$_4$−Ti was revealed by XRD analysis (Figure 2). Low-angle XRD pattern of CuPcS$_4$−Ti exhibited a typical hexagonal ($p6mm$) mesophase, with a main peak observed at $2\theta = 0.79°$ indexed on a hexagonal lattice as the (100) reflection (d_{100} = 11.2 nm) and two small peaks at $2\theta = 1.37$ and $1.58°$, which could be indexed on a hexagonal lattice as (110) and (200) reflections. The unit-cell parameter (a) was calculated to be 12.9 nm. One broad peak ranged from $2\theta = 15-35°$ was observed in the wide-angle XRD pattern (see Figure S2 in the Supporting Information), indicating the low crystallinity of the as-prepared CuPcS$_4$−Ti, which was caused by the extensive condensation of coupling CuPcS$_4$ molecules with Ti^{4+} ions leaving scarce large titania crystals (26, 27). The ordered mesoporous structure was also confirmed by the TEM observations. Micron-scaled nanoparticles with mesopores assembled together irregularly (Figure S3 in Supporting Information). In the magnified images (Figure 3), the hexagonal arrangement of the mesopores could be clearly seen with the average pore size of around 9.5 nm and the pore wall thickness of 3.4 nm (Figure 3a), which are of the similar sizes of the previously reported mesoporous silicas prepared in the presence of triblock copolymer (17, 28). Typical one-dimensional (1D) channels were observed from
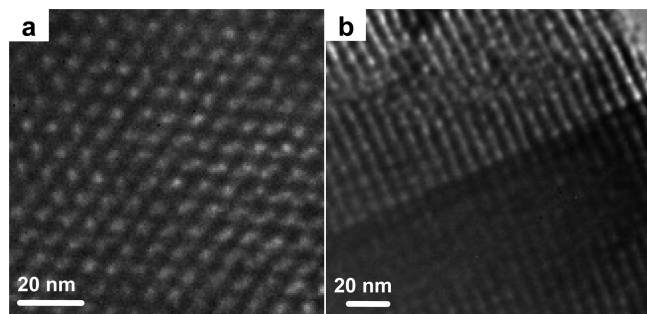
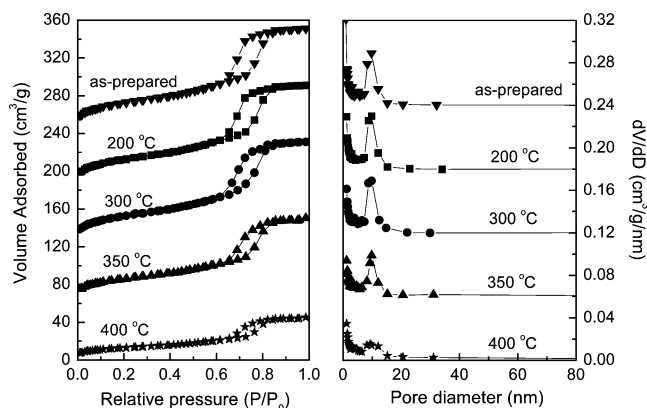FIGURE 3. TEM images of the synthesized CuPcS$_4$–Ti sample.

FIGURE 4. N$_2$ adsorption–desorption isotherms (left) and the corresponding pore size distribution curves (right) determined by BJH method of the as-prepared CuPcS$_4$–Ti and the calcined samples at different temperatures.

tant extraction was calcined in the air at 200, 300, 350, and 400 °C. The N$_2$ sorption isotherms of the calcined CuPcS$_4$–Ti samples were still of type IV with type H1 hysteresis (Figure 4). One narrow peak around 9.5–9.6 nm could be observed in the pore size distribution curves even after calcination at 350 °C, whereas the pore size distribution of the 400 °C-calcined sample was poor. The surface areas and pore volumes of the samples calcined at 200 and 300 °C were hardly changed in comparison with the as-prepared CuPcS$_4$–Ti sample, whereas these values got a sharp decrease when calcined at 350 and 400 °C (Table 1). In the low-angle XRD patterns of the calcined samples (Figure 2), both the main peak of (100) reflection and two small peaks of (110) and (200) reflections could be well-preserved when the sample calcined at 300 °C. But the (110) and (200) reflections appeared to be weak when calcined at 350 °C, and only one broad peak could be observed after calcination at 400 °C. This indicated that the ordered mesoporous structure could be thermally stable up to around 350 °C, and the regularity of the mesopores gradually deteriorated when the calcination temperature was further increased. The wide angle XRD patterns (see Figure S2 in the Supporting Information) still indicated the low crystallinity of the calcined samples. Because the organic moiety of CuPcS$_4$ bridged molecules began to decompose at 328 °C, it is thus indicated that the present CuPcS$_4$–Ti materials could be stable to around 328 °C with the hybrid framework and ordered mesopores well-preserved.

the side view of the CuPcS$_4$–Ti sample (Figure 3b). The N$_2$ sorption isotherm of CuPcS$_4$–Ti is of type IV, characteristic of mesoporous materials, according to the IUPAC classification (Figure 4) (29). Type H1 hysteresis loop was observed, exhibiting parallel branches, which was often reported for materials with cylindrical pore geometry and a high degree of pore size uniformity with facile pore connectivity (29). One narrow peak around 9.5 nm was observed in the pore size distribution curve, consistent with TEM observations. And the surface area and pore volume were 164 m^2/g and 0.33 cm^3/g, respectively (Table 1).

To further test the thermal stability of the ordered mesostructure, the as-prepared CuPcS$_4$–Ti sample after surfac-

In the FT-IR spectrum of the CuPcS$_4$–Ti sample (Figure 5), almost every band of CuPcS$_4$ molecule was well-preserved with only slight strength change. Noticeably, the bands at 1034 and 1182 cm^{-1}, assigned as the symmetric and asymmetric stretching vibrations in O=S=O respectively (30), weakened dramatically, which could be attributed to the extensive condensation of CuPcS$_4$ with titanium to form the S–O···Ti bonding mode. Correspondingly, a new band at 1395 cm^{-1} appeared on the spectrum of CuPcS$_4$–Ti, which is the typical absorption band of S–O···Ti stretching vibrations (31). The low-frequency bands in the range <500 cm^{-1} corresponds to the Ti–O–Ti

Table 1. Summary of the Physicochemical Properties of As-Prepared CuPcS$_4$–Ti Material and the Samples Calcined at Different Temperatures

Ti/CuPcS$_4$ molar ratio	sample	S_{BET}[a] (m^2/g)	$D_{BJH-ads}$[b] (nm)	D_{ave}[c] (nm)	V_{pore}[d] (cm^3/g)	mesophase	photoelectric conversion efficiency (η, %)[e]
	as-prepared	164	9.5	11.2	0.33	hexagonal	0.53
	200 °C calcined	162	9.5	11.3	0.33	hexagonal	
	300 °C calcined	159	9.5	11.3	0.32	hexagonal	
50	350 °C calcined	131	9.5	11.5	0.24	hexagonal (weak)	
	400 °C calcined	65	9.6	11.7	0.14	irregular	
	mesostructure-destroyed	28					0.23
	CuPcS$_4$ modified TiO$_2$	169					0.004
49	as-prepared	170	9.5	11.6	0.34	hexagonal	0.49
51	as-prepared	165	9.7	11.6	0.33	hexagonal	0.52
52	as-prepared	161	9.8	11.9	0.32	hexagonal	0.51

[a] BET surface area calculated from the linear part of the BET plot. [b] Estimated using the adsorption branch of the isotherms by the BJH method. [c] Average pore size. [d] Single point total pore volume of pores at $P/P_0 = 0.98$. [e] Total photoelectric conversion efficiency under simulated sunlight irradiation.
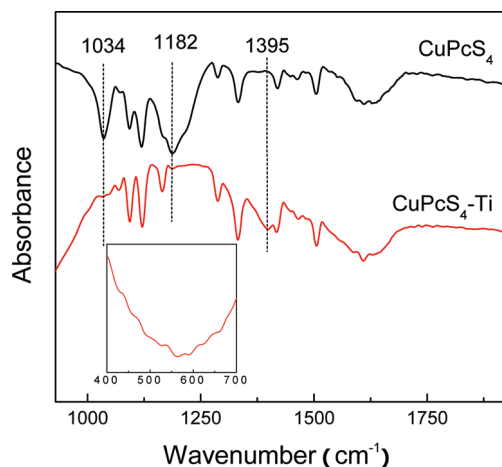
FIGURE 5. FT-IR spectra of the CuPcS₄—Ti sample and CuPcS₄.

vibration of TiO_2 was very weak in the spectrum of CuPcS$_4$—Ti (Figure 5 inset) (32), indicating Ti atoms were linked to CuPcS$_4$ molecules through S—O···Ti bonds instead of forming large TiO_2 aggregates. ICP emission spectroscopy was employed to analyze chemical compositions of the resultant solids (48.63% Ti, 1.29% Cu in mass), revealing the Ti/Cu molar ratio approximate to 50 in the sample, namely, the Ti/CuPcS$_4$ molar ratio approximate to 50.

Figure 6 shows the high-resolution XPS spectra of Ti 2p, O 1s, and S 2p, taken on the surface of CuPcS$_4$—Ti sample, which are collected to study the surface chemistry of the synthesized material. The surface atomic composition of the materials was calculated from the XPS spectra, showing 0.45% Cu, 1.80% S, and 22.42% Ti. The Ti/Cu molar ratio was of 50, which was identical to that of the ICP results, indicating the compositional homogeneity throughout the hybrid material. The Ti 2p line of CuPcS$_4$—Ti sample is composed of two single peaks situated at 458.2 eV for Ti 2p$_{3/2}$ and 463.8 eV for Ti 2p$_{1/2}$, indicating that the Ti element mainly exists as the chemical state of Ti^{4+} (33, 34). Compared with the binding energy of pure TiO_2 (459 eV for Ti2p$_{3/2}$ and 464.8 eV for Ti2p$_{1/2}$), the binding energy of main Ti 2p decreases in the titanium sulfonate hybrid, which is the result from the organosulfonate incorporation into the titania network, similar to some metal phosphonate materials (35, 36). Curve-fitting result of the high-resolution spectrum of O 1s photoelectron peak suggested that there should exist three kinds of oxygen. The main peak at around 530.5 eV can be attributed to the oxygen in Ti—O—S linkages (37), whereas the peak at around 532.0 eV can be assigned to surface hydroxyl (38). A small amount of Ti—O—Ti linkages was detected at 529.6 eV, whereas no peak corresponding to S—O—S linkages at around 531.5 eV could be found, indicating there existed scarce condensation of the neighboring dye molecules (39). A very symmetrical peak centered at 168.3 eV was detected in the S 2p spectrum, showing an negative shift compared with the sulfur in a hexavalent oxidation state (S^{6+}, ~169 eV) (40). The difference of the S 2p binding energy indicated that the presence of the S—O···Ti bonds which resulted in the change of the chemical circumstance of sulfur, and thus the S atoms of dye
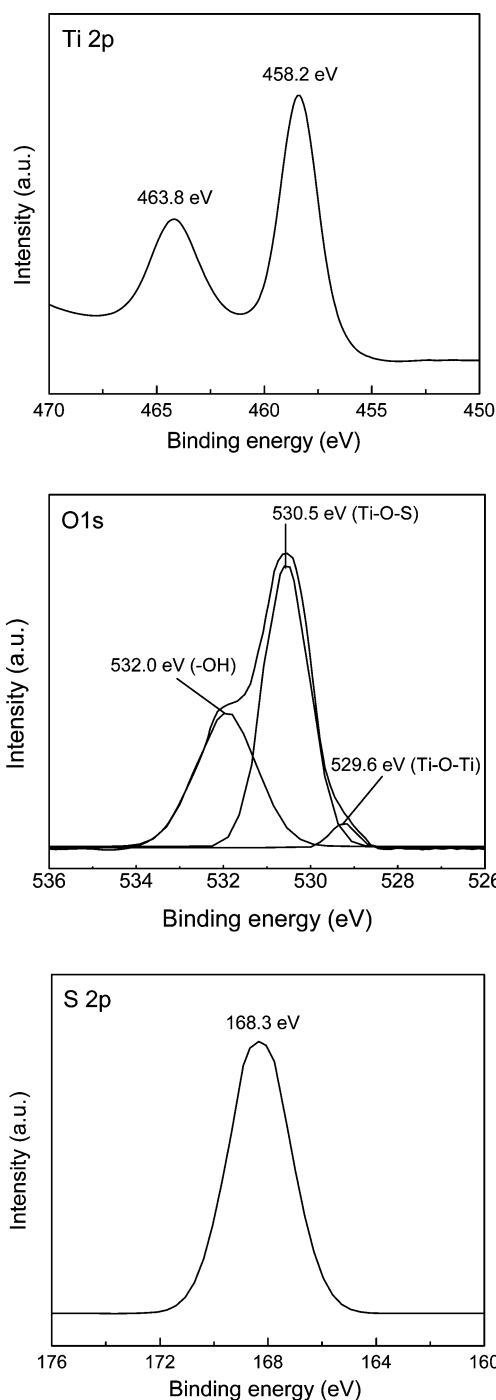

FIGURE 6. High-resolution XPS spectra of the Ti 2p, O 1s, and S 2p regions of the synthesized CuPcS₄—Ti material.

molecules could mainly coordinate with Ti^{4+} species in the network which is in well accordance with the FT-IR results. Based on TGA-DSC, IR, XPS, and XRD measurements, the ideal skeletal structure of the synthesized CuPcS$_4$—Ti material was proposed, shown in Figure 7. The CuPcS$_4$ coupling groups were dispersed homogeneously within the organic—inorganic hybrid network, covalently bonded with Ti^{4+} through the S—O···Ti mode, whereas the Ti^{4+} ions were coordinated with organic motifs in the form of TiO$_4$ oligomers instead of large titania crystals. Thus the central copper-phthalocyanine groups were efficiently isolated from each other by the surrounding inorganic species. All these
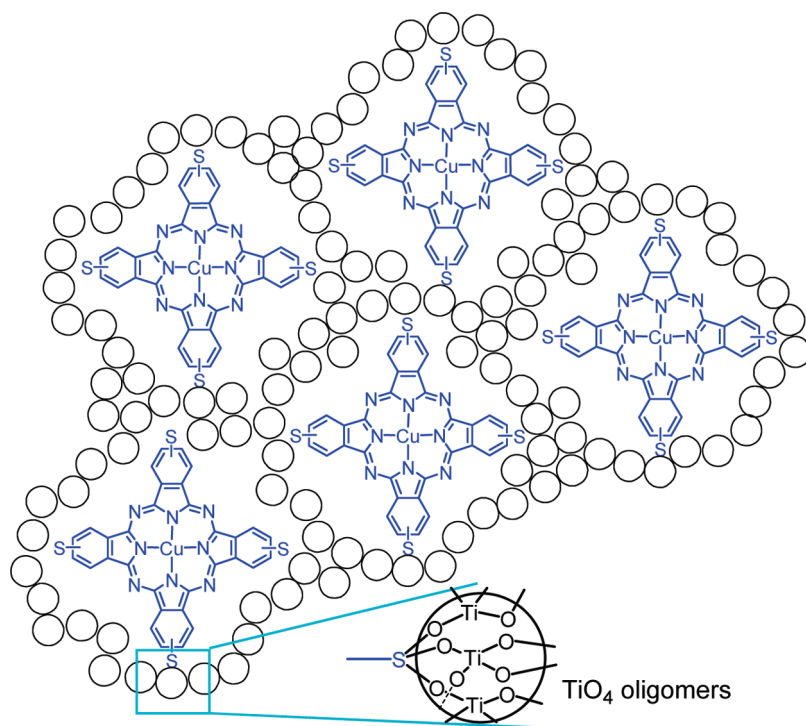
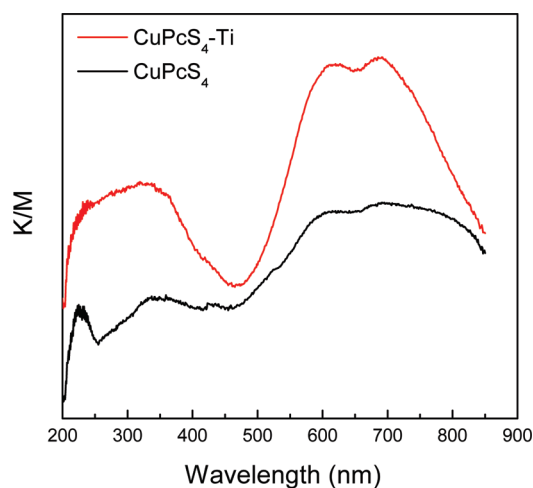FIGURE 7. Proposed skeletal structure of the synthesized CuPcS$_4$−Ti material.

FIGURE 8. UV−vis diffuse reflectance spectra of the CuPcS$_4$−Ti sample and CuPcS$_4$.

make a bimetallic and large conjugated hybrid framework for the ordered hexagonal mesophase, and it was the first reported ordered mesoporous metal sulfonate material to the best of our knowledge.

3.2. Photoelectric Conversion. UV−vis diffuse reflectance spectroscopy has been performed to assess the optical properties and electronic structure of the synthesized CuPcS$_4$−Ti sample (Figure 8). Similar tendency of the as-prepared sample and pure CuPcS$_4$ was obtained in the wavelength range from 200 to 800 cm^{-1}. Interestingly, two absorption peaks at around 250−390 cm^{-1} and 580−750 cm^{-1} in ultraviolet and visible light areas, respectively, were very outstanding for CuPcS$_4$−Ti, which were much higher than those of pure organic CuPcS$_4$ molecules. This phenomena could be attributed to the strong interactions between the organic and inorganic moieties in the hybrid sulfonate

framework, which has been observed in the optical properties of some previously reported phosphonate-based hybrid materials (26, 35, 41).

Large π-aromatic molecules, such as porphyrins, phthalocyanines, and perylenes, have been widely used in the highly efficient dye-sensitized solar cells, because of their photostability and high light-harvesting capabilities that can allow applications in thinner, low-cost dye-sensitized solar cells. Phthalocyanines exhibit strong absorption around 300 and 700 nm and redox features that are similar to porphyrins. Moreover, phthalocyanines are transparent over a large region of the visible spectrum, thereby enabling the possibility of using them as "photovoltaic windows" (12). The traditional preparation strategy of electrodes of dye sensitized solar cell was by adsorption of dye molecules onto the presynthesized semiconductor films (42). For the present CuPcS$_4$−Ti coated electrode, the dye molecules were linked to Ti atoms through the S−O···Ti covalent bonds, which could largely enhance the interactions between sensitizers and the semiconductor, and decrease the loss of dye molecules during the application of the solar cells. The utilization of commercially available CuPcS$_4$ as dye molecule and graphite rods as the counter electrode, and the simple one-step coating process of the synthesized mesoporous CuPcS$_4$−Ti materials onto the conductive glass lead to the low cost and practicality of this self-made solar cell. The configuration of the cell was shown in Figure S1 in the Supporting Information. To investigate the cell performance, current−voltage characteristics were measured under the simulated sunlight irradiation (Figure 9). Short-circuit photocurrent density (J_{sc}), open circuit potential (V_{oc}), fill factor (ff), and overall conversion efficiency (η) of the self-made solar cell were summarized in Table S1 (Supporting Infor-
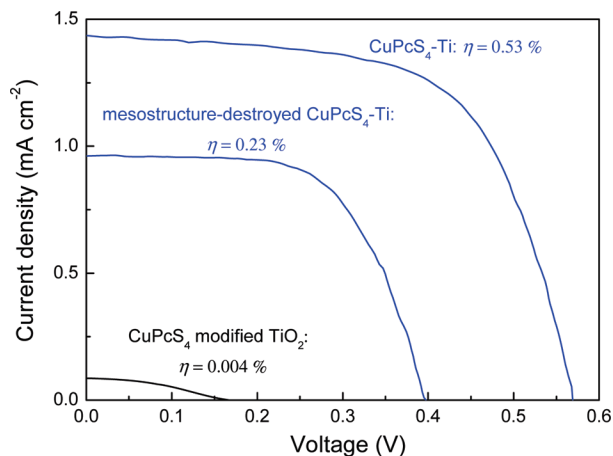
FIGURE 9. Current−voltage characteristics of the mesoporous CuPcS$_4$−Ti-based solar cell under simulated sunlight irradiation.

mation). The conversion efficiency (η) of CuPcS$_4$−Ti hybrids was calculated to be 0.53 %, which was relatively high compared with the reported phthalocyanine sensitized solar cells. For example, a combination of catechol axial attachment to a TiO$_2$ surface, followed by the ligation to titanium(IV) tetra(*tert*-butyl)phthalocyanine without the use of coadsorbents, with the bulky *tert*-butyl peripheral groups allowed for selective electron injection into the TiO$_2$ by Soret band excitation, but the η value was 0.2 % (9). Novel highly substituted zinc phthalocyanine carboxylic acid Zn-9 was used for dye-sensitized solar cells, in which the aggregation tendency of phthalocyanines could be effectively suppressed by the high degree of substitutions, leading to a η value of 0.57 % (6). The highest power conversion efficiency among the reported phthalocyanine-sensitized TiO$_2$ cell was achieved by Nazeeruddin and Torres et al. (10, 11) Their cell performance was aided with the coadsorption of chenodeoxycholic acid that is well-known to suppress the dye aggregation on the TiO$_2$ surface. They prepared a novel unsymmetrical zinc phthalocyanine sensitizer Zn-8 with the same three *tert*-butyl and one carboxylic acid group that act as "push" and "pull" groups, respectively, and the η value was determined to be up to 3.5 %. To the best of our knowledge, this is one of the scarce examples that have a much higher η value than the present CuPcS$_4$−Ti-based cell. Although some of these mentioned phthalocyanine sensitized solar cells have better performance than our CuPcS$_4$−Ti-based solar cell, the complex preparation process of the highly substituted phthalocyanines and the use of expensive unsymmetrical phthalocyanines still limit their application areas, and it is very valuable to access the high conversion efficiency by using low-cost and commercially available dye molecules. The stability for CuPcS$_4$−Ti (Ti/CuPcS$_4$ molar ratio of 50)-based solar cells was measured within 20 h, and the conversion efficiency shows no obvious drop after 20 multiple use cycles (see Figure S4 in the Supporting Information) with the relative standard deviation (RSD) of 1.92 %. The batch to batch reproducibility was measured by fabricating 5 solar cells from CuPcS$_4$−Ti materials synthesized individually with the same method, and the RSD was comfirmed to be 3.37 %.

All these indicated that the present CuPcS$_4$−Ti-based solar cells have well stability and reproducibility.

To confirm the superiority of organic−inorganic hybrid sulfonate materials as electrodes, we prepared a common dye-sensitized electrode by adsorption of CuPcS$_4$ onto mesoporous titania membrane, and the molar ratio of Ti/CuPcS$_4$ was adjusted to be around 50. The conversion efficiency was calculated to be 0.004 %, which was much lower than that of CuPcS$_4$−Ti-based hybrid materials. For the present organosulfonate materials, the sulfonate groups were homogenously bonded into the hybrid framework, which prevents the formation of large titania aggregates that could be detected by XRD and FT-IR analysis, similar to the cases in metal phosphonate materials (26, 43). The inorganic moiety surrounded CuPcS$_4$ centers mainly existed in the form of TiO$_4$ oligomers, which acted as the electron acceptors. Electron injection into the conduction band (CB) of TiO$_4$ occurred from the first excited singlet state (S$_1$) of CuPcS$_4$ instead of from the first excited triplet state (T$_1$), which is a usual mechanism in dye sensitization of TiO$_2$ with phthalocyanines (44), shown in Figure S5 (Supporting Information). The large conjugated system of CuPcS$_4$ molecules could be elongated probably through the participation of sulfur *d*-orbit into the π system of the connected benzene (45), which acted as both bridging and binding moieties. Generally, this one-pot strategy of condensing TiCl$_4$ with CuPcS$_4$ would lead to the molecular-level penetration of large π-aromatic groups into the semiconductor network with limited polymerization degree (TiO$_4$ oligomers), and the high contact and utilization of organic dyes and the semiconductors in the hybrid materials would contribute to improve the photoelectric conversion efficiency. First, the isolation of copper-phthalocyanine centers by the surrounding TiO$_4$ oligomers could effectively suppress the aggregation of CuPcS$_4$ dyes that may decrease the conversion effeciency in some traditional dye-sensitized solar cells (12). The high loading amount of dyes was achieved by this method, while the self-quenching of the phthalocyanine excited singlet state caused by dye aggregation in the traditionally prepared electrodes was unavoidable (12), which could explain the low conversion efficiency in the synthesized CuPcS$_4$ modified TiO$_2$ sample (0.004 %). We also decreased the CuPcS$_4$ content to Ti/CuPcS$_4$ molar ratio of 500 for the CuPcS$_4$ modified titania sample, but conversion efficiency was still low (<0.01 %) because of the dye aggregation. In fact, the dye concentrations of the reported dye-sensitized titania membranes were usually very low. For example, Eu et al. reported phthalocyanine-sensitezed solar cells with the dye content of 1.4 × 10^{-10} mol/cm^2 (6). There is another important potential for the high dye concentration of the present sulfonate-based solar cells, that the dye content in the hybrid materials could be adjusted in a very wide range simply through changing the adding amounts of raw materials (TiCl$_4$ and CuPcS$_4$), which means the photoelectric conversion efficiency could be further promoted facilely.

Many factors could determine the photoelectric conversion efficiency of the CuPcS$_4$−Ti based solar cell. For ex-
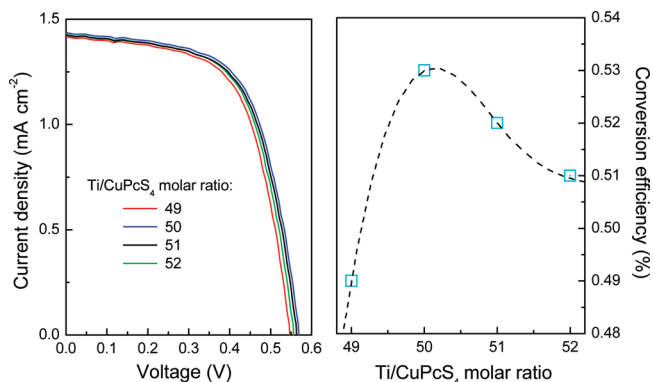
FIGURE 10. Current–voltage characteristics of the mesoporous CuPcS$_4$–Ti based solar cells with different Ti/CuPcS$_4$ molar ratios.

ample, the ordered mesoporous structure of CuPcS$_4$–Ti material was destroyed by the ball milling technique (46), which lead to the sharp decreasing of the specific surface to 28 m^2/g. Also testing under simulated sunlight irradiation, the conversion efficiency was decreased to 0.23%, that is 43% of the initial efficiency (Figure 9). This results suggested that the ordered mesoporous hybrid materials with high surface area and pore volume could enhance the photoelectric conversion efficiency, probably due to the large contact area to lights and efficient transmission of photoelectrons. Another important factor was the contents of the organic dye used in the hybrid membrane. By slightly adjusting the adding amounts of the raw materials, we have prepared a series of ordered mesoporous CuPcS$_4$–Ti materials with the Ti/CuPcS$_4$ molar ratio of 49, 51, and 52, besides the above-mentioned CuPcS$_4$–Ti with Ti/CuPcS$_4$ molar ratio of 50, and the pore structure of these materials were quite similar, shown in Table 1, see Figures S6 and S7 in the Supporting Information. The current–voltage characteristics were measured (Figure 10), giving the sequence of CuPcS$_4$–Ti (50) > CuPcS$_4$–Ti (51) > CuPcS$_4$–Ti (52) > CuPcS$_4$–Ti (49) (Table 1). Thus it is concluded that the photoelectric conversion efficiency was not positive correlated to dye content, and the efficiency reached its highest value at Ti/CuPcS$_4$ = 50 under the present experimental condition. In other words, the conversion efficiency of the solar cell is related to the relative content of CuPcS$_4$ centers to the surrounding TiO$_4$ oligomers, which could be easily adjusted in the preparation process.

The current–voltage characteristics were also measured under the irradiation of four different monochromatic light sources (see Figure S8 in the Supporting Information). The conversion efficiency gave the following sequence: 2.57% (red light) > 2.38% (UV light) > 0.45% (green light) > 0.33% (blue light). This sequence was consistent to the observation of UV–vis diffuse reflectance spectroscopy with two strong absorption peaks in UV and red light regions and very low adsorption in blue region, which also confirmed that the phthalocyanine is indeed the main source of the photocurrent generation. The distinct photoelectric conversion efficiencies under different light sources make the mesoporous CuPcS$_4$–Ti materials possibly practical in some photodetector applications. Similarly, the mesostructure-destroyed

CuPcS$_4$–Ti and the CuPcS$_4$-modified TiO$_2$ samples exhibited much lower η values. As shown in Figure S9 in the Supporting Information, the current–voltage characteristics of the synthesized samples with different Ti/CuPcS$_4$ molar ratios were measured under red light irradiation, giving the sequence of CuPcS$_4$–Ti (50) > CuPcS$_4$–Ti (51) > CuPcS$_4$–Ti (52) > CuPcS$_4$–Ti (49), which was the same to that under simulated solar light irradiation. It is theoretically possible that the conversion efficiency could be extended to a much wider range by further changing the Ti/CuPcS$_4$ molar ratio. Detailed experimental investigation at other factors that determine the conversion efficiency, such as the thickness of the hybrid film, the concentration of the electrolyte, and the pore size of the sensitized materials, are still being taken in our laboratory.

4. CONCLUSIONS

Hexagonal mesoporous titanium tetrasulfonate materials with an average pore size of around 9.5 nm were synthesized by a simple autoclaving method in the presence of surfactant F127. The CuPcS$_4$ coupling groups were dispersed homogeneously within the inorganic–organic hybrid network, covalently bonded with Ti through the S–O···Ti mode, whereas the Ti ions were almost tetrahedral coordinated with organic motifs instead of forming large titania aggregates. All these make a bimetallic and large conjugated hybrid framework for the ordered hexagonal mesophase, which is beneficial to the photoelectric conversion. It was proved that the synthesized mesoporous CuPcS$_4$–Ti was useful as the electrode materials, exhibiting high conversion efficiency under simulated sunlight irradiation. The next attempts would focus on improving the crystallinity of mesoporous walls and adjusting the dye content and pore size of the metal sulfonate materials, and on further increasing of the photoelectric conversion efficiency of the mesoporous CuPcS$_4$–Ti based solar cell.

Supporting Information Available: Photovoltaic parameters of the CuPcS$_4$–Ti solar cell; the structure of copper(II) phthalocyanine-tetrasulfonic acid tetrasodium salt; the configuration of the self-made solar cell; wide-angle XRD patterns of the as-prepared CuPcS$_4$–Ti and calcined samples at different temperatures; the TEM image of the synthesized CuPcS$_4$–Ti sample with low magnification; stability testing of the conversion efficiency for CuPcS$_4$–Ti-based solar cells; schematic representation of energy levels of the CuPcS$_4$–Ti coated photoelectrode; N$_2$ sorption and XRD patterns of the CuPcS$_4$–Ti samples with different Ti/CuPcS$_4$ molar ratios; and current–voltage characteristics of the mesoporous

CuPcS$_4$−Ti-based solar cell under monochromatic light sources (PDF). This material is available free of charge via the Internet at http://pubs.acs.org/.

REFERENCES AND NOTES

(1) Youngblood, W. J.; Lee, S. H. A.; Maeda, K.; Mallouk, T. E. *Acc. Chem. Res.* **2009**, *42*, 1966.
(2) Concepcion, J. J.; Jurss, J. W.; Brennaman, M. K.; Hoertz, P. G.; Patrocinio, A. O. T.; Iha, N. Y. M.; Templeton, J. L.; Meyer, T. J. *Acc. Chem. Res.* **2009**, *42*, 1954.
(3) Ali, H.; van Lier, J. E. *Chem. Rev.* **1999**, *99*, 2379.
(4) Peng, X. S.; Jin, J.; Ericsson, E. M.; Ichinose, I. *J. Am. Chem. Soc.* **2007**, *129*, 8625.
(5) Hasobe, T.; Imahori, H.; Yamada, H.; Sato, T.; Ohkubo, K.; Fukuzumi, S. *Nano Lett.* **2003**, *3*, 409.
(6) Eu, S.; Katoh, T.; Umeyama, T.; Matano, Y.; Imahori, H. *Dalton Trans.* **2008**, 5476.
(7) Giraudeu, A.; Fan, F. R. F.; Bard, J. *J. Am. Chem. Soc.* **1980**, *102*, 5137.
(8) He, J.; Hagfeldt, A.; Lindquist, S. E.; Grennberg, H.; Korodi, F.; Sun, L.; Åkermark, B. *Langmuir* **2001**, *17*, 2743.
(9) Palomares, E.; Martinez-Díaz, M. V.; Haque, S. A.; Torres, T.; Durrant, J. R. *Chem. Commun.* **2004**, 2112.
(10) Cid, J. J.; Yum, J. H.; Jang, S. R.; Nazeeruddin, M. K.; Martínez-Ferrero, E.; Palomares, E.; Ko, J.; Grätzel, M.; Torres, T. *Angew. Chem., Int. Ed.* **2007**, *46*, 8358.
(11) Yum, J. H.; Jang, S. R.; Humphry-Baker, R.; Grätzel, M.; Cid, J. J.; Torres, T.; Nazeeruddin, M. K. *Langmuir* **2008**, *24*, 5636.
(12) Imahori, H.; Umeyama, T.; Ito, S. *Acc. Chem. Res.* **2009**, *42*, 1809.
(13) Shimizu, G. K. H.; Vaidhyanathan, R.; Taylor, J. M. *Chem. Soc. Rev.* **2009**, *38*, 1430.
(14) Gándara, F.; García-Cortés, A.; Cascales, C.; Gómez-Lor, B.; Gutiérrez-Puebla, E.; Iglesias, M.; Monge, A.; Snejko, N. *Inorg. Chem.* **2007**, *46*, 3475.
(15) Côté, A. P.; Shimizu, G. K. H. *Inorg. Chem.* **2004**, *43*, 6663.
(16) Chandler, B. D.; Cramb, D. T.; Shimizu, G. K. H. *J. Am. Chem. Soc.* **2006**, *128*, 10403.
(17) Zhao, D. Y.; Feng, J. L.; Huo, Q. S.; Melosh, N.; Fredrickson, G. H.; Chmelka, B. F.; Stucky, G. D. *Science* **1998**, *279*, 548.
(18) Davis, M. E. *Nature* **2002**, *417*, 813.
(19) Dai, S.; Burleigh, M. C.; Shin, Y.; Morrow, C. C.; Barnes, C. E.; Xue, Z. *Angew. Chem., Int. Ed.* **1999**, *38*, 1235.
(20) Cao, J. L.; Wang, Y.; Zhang, T. Y.; Wu, S. H.; Yuan, Z. Y. *Appl. Catal., B* **2008**, *78*, 120.
(21) Agarwala, S.; Kevin, M.; Wong, A. S.; Peh, C. K.; Thavasi, V.; Ho, G. W. *ACS Appl. Mater. Interfaces* **2010**, *2*, 1844.
(22) Bisquert, J.; Cahen, D.; Hodes, G.; Rühle, S.; Zaban, A. *J. Phys. Chem. B* **2004**, *108*, 8106.
(23) Kartini, I.; Menzies, D.; Blake, D.; da Costa, J. C. D.; Meredith, P.; Riches, J. D.; Lu, G. Q. *J. Mater. Chem.* **2004**, *14*, 2917.
(24) Côté, A. P.; Shimizu, G. K. H. *Chem. Commun.* **2001**, 251.
(25) Ma, T. Y.; Zhang, X. J.; Yuan, Z. Y. *J. Phys. Chem. C* **2009**, *113*, 12854.
(26) Ma, T. Y.; Zhang, X. J.; Yuan, Z. Y. *J. Mater. Sci.* **2009**, *44*, 6775.
(27) Haskouri, J. EI.; Guillem, C.; Latorre, J.; Beltrán, A.; Beltrán, D.; Amorós, P. *Chem. Mater.* **2004**, *16*, 4359.
(28) Zhao, D. Y.; Huo, Q. S.; Feng, J. L.; Chmelka, B. F.; Stucky, G. D. *J. Am. Chem. Soc.* **1998**, *120*, 6024.
(29) Kruk, M.; Jaroniec, M. *Chem. Mater.* **2001**, *13*, 3169.
(30) Lu, A. H.; Tüysüz, H.; Schüth, F. *Microporous Mesoporous Mater.* **2008**, *111*, 1173.
(31) Platero, E. E.; Mentruit, M. P.; Aréan, C. O.; Zecchina, A. *J. Catal.* **1996**, *162*, 268.
(32) Soler-Illia, G. J. A. A.; Louis, A.; Sanchez, C. *Chem. Mater.* **2002**, *14*, 750.
(33) Losito, I.; Amorisco, A.; Palmisano, F.; Zambonin, P. G. *Appl. Surf. Sci.* **2005**, *240*, 180.
(34) Biener, J.; Baumer, M.; Wang, J.; Madrix, R. J. *Surf. Sci.* **2000**, *450*, 12.
(35) Zhang, X. J.; Ma, T. Y.; Yuan, Z. Y. *J. Mater. Chem.* **2008**, *18*, 2003.
(36) Zhang, X. J.; Ma, T. Y.; Yuan, Z. Y. *Eur. J. Inorg. Chem.* **2008**, 2721.
(37) Liu, Y.; Liu, J.; Lin, Y.; Zhang, Y.; Wei, Y. *Ceram. Int.* **2009**, *35*, 3061.
(38) Xu, Z. L.; Shang, J.; Liu, C. M.; Kang, C. L.; Guo, H. C.; Du, Y. G. *Mater. Sci. Eng., B* **1999**, *63*, 211.
(39) Xie, C.; Xu, Z. L.; Yang, Q. J.; Xue, B. Y.; Du, Y. G.; Zhang, J. H. *Mater. Sci. Eng., B* **2004**, *112*, 34.
(40) Raj, K. J. A.; Wiswanathan, B. *ACS Appl. Mater. Interf.* **2009**, *1*, 2462.
(41) Ma, T. Y.; Zhang, X. J.; Yuan, Z. Y. *Microporous Mesoporous Mater.* **2009**, *123*, 234.
(42) Sayama, K.; Sugihara, H.; Arakawa, H. *Chem. Mater.* **1998**, *10*, 3825.
(43) Ma, T. Y.; Yuan, Z. Y. *Chem. Commun.* **2010**, *46*, 2325.
(44) Nazeeruddin, M. K.; Humphry-Baker, R.; Grätzel, M.; Wöhrle, D.; Schnurpfeil, G.; Schneider, G.; Hirth, A.; Trombach, N. *J. Porphyrins Phthalocyanin.* **1999**, *3*, 230.
(45) Oda, M.; Sato, N. *J. Phys. Chem. A* **1998**, *102*, 3283.
(46) A ball mill, a cylindrical device containing different materials used as media including ceramic balls, flint pebbles, and stainless steel balls, is used to grind materials into extremely fine powder. Suryanarayana, C. *Prog. Mater. Sci.* **2001**, *46*, 1.

AM100741U